COMMUNICATIONS IN SCIENCE AND TECHNOLOGY
Homepage: cst.kipmi.or.id

Oxygen-functionalized carbon nanofibers from kulim wood for high-performance supercapacitors via an integrated chemical–physical catalyst approach

Erman Taer[a,*], Apriwandi[a], Ebigail Nur Tabita Tambunan[a], Novi Yanti[a], Nursyafni[a], Rika Taslim[b]

[a]*Department of Physics, University of Riau, Riau 28293 Indonesia*
[b]*Department of Industrial Engineering, Universitas Islam Negeri Sultan Syarif Kasim Riau, 28293 Indonesia*

Article history:
Received: 13 November 2025 / Received in revised form: 15 December 2025 / Accepted: 17 December 2025

Abstract

This study highlights the critical role of oxygen-functionalized hierarchical nanofiber structures derived from kulim wood waste in improving the electrochemical performance of symmetric supercapacitors. A one-step catalyst-assisted method was developed to synthesize these carbon nanofibers. The synthesized material exhibited well-defined oxygen functionalities (9.34% oxygen content) and exceptional porosity (1070 m^2/g), demonstrating a micro-mesoporosity ratio of nearly 4:1. This structural design led to enhanced capacitive properties, achieving a capacity of 172 F/g in acid media and a rate capability of 81.2% at 10 A/g. The oxidation reactions indicated a mixed energy storage mechanism, with 83% EDL-controlled and 22% redox-controlled processes. Additionally, the material showed an energy output of 19.91 Wh/kg and a power density of 1.02 kW/kg, showcasing its potential for sustainable energy storage applications. Importantly, this work offers a scalable, low-cost, and biomass-driven strategy for producing high-performance carbon electrodes, advancing sustainable supercapacitor technologies.

Keywords: Oxygen-functionalized; nanofiber; porous carbon; electrode material; supercapacitor

1. Introduction

The growing global demand for energy and the adverse effects of CO_2 emissions have intensified the pursuit of environmentally friendly and sustainable renewable energy solutions. Renewable energy sources are projected to account for the majority of the global energy demand growth, with an annual increase of approximately 23% [1]. However, the success of this energy transition critically depends on advances in energy storage technologies, which serve as essential components in stabilizing intermittent renewable power systems. Among these technologies, supercapacitors have emerged as promising candidates due to their long operational lifespan, high power density, rapid charge–discharge response, and cost-effective production [2,3]. Despite these advantages, their relatively low energy density remains a major limitation compared to batteries [4].

Several types of electrode materials, including polymers, metal oxides, and graphene-based hybrids, have demonstrated energy storage capabilities comparable to those of lithium-ion batteries [5,6]. However, their large-scale applications are often constrained by issues such as high cost, limited raw material availability, poor cycling stability, and potential environmental toxicity. In contrast, carbon-based materials have gained wide attention owing to their abundant availability, low cost, tunable porosity, superior electrical conductivity, and excellent electrochemical stability [7,8]. Among them, biomass-derived carbon has emerged as a sustainable and efficient electrode material due to its natural abundance and hierarchical structure. Biomass carbons typically exhibit large surface areas (>3000 m^2/g), interconnected three-dimensional (3D) pore architectures, and high structural adaptability at the nanoscale [9–11]. Nevertheless, most of these materials rely primarily on the electric double-layer capacitance (EDLC) mechanism, which limits their practical performance. A large surface area alone does not guarantee high-rate capability, as excessive microporosity may hinder ion transport and reduce electrical conductivity.

To overcome these constraints, heteroatom doping, particularly oxygen functionalization, has recently been recognized as an effective strategy to introduce additional pseudocapacitance through reversible redox reactions, thereby enhancing the overall energy density [12,13]. Oxygen functionalities not only contribute to Faradaic reactions but

* Corresponding author.
Email: erman.taer@lecturer.unri.ac.id
https://doi.org/10.21924/cst.10.2.2025.1834

also improve surface wettability and interfacial ion diffusion. For example, Atika and Dutta (2021) synthesized oxygen-functionalized carbon from eucalyptus wood with a surface area of 1032 m²/g and 18.61% oxygen content, achieving 322 F/g and 40.5 Wh/kg [14]. Likewise, Al and Kabakcı (2024) used oxygen-rich hazelnut shells to obtain porous carbon with a specific capacitance of 319 F/g and a surface area of 1052 m²/g [15]. These findings demonstrate that high surface area alone is not the sole determinant of performance; rather, the synergy between hierarchical porosity and oxygen functional groups plays a crucial role [16–18]. Oxygen functionalities can enhance electrochemical activity and serve as stable anchoring sites for other redox-active species, thereby improving both energy density and cycling stability [19,20]. However, the introduction of oxygen species may reduce electrical conductivity, creating a trade-off between capacitance enhancement and electron transport efficiency. To address this, nanostructural engineering such as developing carbon nanofibers has been proposed to provide continuous conductive pathways, ensuring efficient charge transfer while maintaining the advantages of oxygen doping [21–23].

Within this framework, kulim wood *(Scorodocarpus borneensis*), a tropical hardwood abundantly found in Southeast Asia, represents a promising and underutilized biomass source for producing advanced carbon materials. Its lignocellulosic composition, naturally rich in nanofibers and oxygenated structures, offers an excellent foundation for fabricating carbon with hierarchical porosity and tailored oxygen functionalities [24,25]. Moreover, the conversion of kulim wood waste into high-value carbon nanostructures aligns with green chemistry principles and circular economy goals.

In this study, kulim wood waste was utilized to synthesize oxygen-functionalized carbon nanofibers for application as symmetric supercapacitor electrodes. Through controlled carbonization and chemical activation, the resulting material exhibited a specific surface area of 1070 m²/g and an oxygen content of 9.34%, predominantly in carbonyl and hydroxyl configurations. The hierarchical micro–mesoporous network enabled efficient ion transport and charge storage, leading to a specific capacitance of 172 F/g at 1 A/g and a rate retention of 81.9% at 10 A/g.

2. Materials and Methods

2.1. Materials

Carbon nanofiber material with oxygen functionality was derived from kulim wood waste or garlic tree (*Scorodocarpus borneensis*), sourced from furniture entrepreneurs in Pekanbaru City, Indonesia. The chemicals used in the process were supplied by various official distributors, featuring confirmed brand products accompanied by analysis certificates from reputable companies such as Merck KGaA and Panreac Química. Key chemicals used include KOH (in pellet form), sulfuric acid (with 95% purity), and polyvinylidene fluoride (in powder form). During pyrolysis, a gas atmosphere was applied, focusing on high-purity carbon dioxide (CO_2) and nitrogen supplied by a local Indonesian gas company.

2.2. Synthesis of carbon nanofiber with oxygen functionality

The synthesis of oxygen-functionalized carbon nanofibers was conducted using an eco-friendly, one-stage integrated chemical–physical activation approach. Kulim wood waste was first air-dried and then subjected to controlled manual combustion in a steel barrel at atmospheric pressure for 2 h to obtain primary charcoal. The resulting charcoal was repeatedly washed with deionized water until the supernatant became clear, in order to remove residual ash and inorganic impurities. The washed charcoal was then dried at 105 °C for 12 h, followed by mechanical milling and sieving to obtain a fine powder with particle sizes below 100 µm. Chemical activation was performed by impregnating the charcoal powder with potassium hydroxide (KOH, analytical grade) at a mass ratio of 1:1 (KOH:charcoal). The impregnation process was carried out in deionized water under continuous magnetic stirring at 85 °C for 120 min using a hotplate stirrer to ensure homogeneous distribution of the activating agent. The resulting slurry was aged at room temperature for 12 h, followed by oven drying at 110 °C to obtain a solid precursor. The dried precursor was further milled and subsequently carbonized and activated via pyrolysis in a horizontal tubular furnace. The furnace temperature was increased from room temperature to 850 °C at a heating rate of 5 °C min^{-1}. High-purity nitrogen (N_2, 99.99%) was introduced at a constant flow rate of 100 mL min^{-1} up to 600 °C to maintain an inert atmosphere. Upon reaching 600 °C, the gas flow was switched to carbon dioxide (CO_2, 99.99%) at the same flow rate to promote physical activation, and the temperature was maintained at 850 °C for 2 h. After pyrolysis, the furnace was naturally cooled to room temperature under continuous N_2 flow for approximately 10 h.To remove residual potassium-containing species and other inorganic impurities, the obtained carbon material was immersed in 1 M HCl solution and stirred for 2 h, followed by repeated washing with deionized water until the filtrate reached neutral pH (≈7). The final oxygen-functionalized carbon nanofibers were dried at 105 °C for 12 h and stored in a desiccator for further characterization and electrochemical testing.

2.3. Physical properties of materials characterization

The microstructure and phase composition of the synthesized carbon materials were analyzed using X-ray diffraction (XRD, instrument: Shimadzu type MAXima_X XRD 7000) over a scanning range of 0° to 100°. Key parameters such as d-spacing, interlayer distance, and crystallite dimensions ($L_{c/a}$) were determined in accordance with standard analytical protocols. Functional group identification was performed using Fourier-transform infrared (FTIR, instrument: Shimadzu-IR-Prestige-21) spectroscopy in the wavenumber range of 4500 to 500 cm^{-1}. The elemental composition and functionalities of the materials were evaluated using energy-dispersive X-ray spectroscopy (EDS, instrument: JEOL-JSM-IT200) in an energy range of 1 to 20 keV. Surface morphology was confirmed using scanning electron microscopy (SEM, instrument: JEOL-JSM-IT200) at an accelerating voltage of 15 keV, with imaging performed at

magnifications corresponding to scales of 500 nm and 1 µm. Finally, the porosity characteristics, including specific surface area, pore size distribution, and total pore volume, were analyzed through nitrogen (N_2) adsorption-desorption isotherms at 77 K with Quantachrome Nova 4200e instrument, using the Brunauer–Emmett–Teller (BET), T-plot, and Barrett–Joyner–Halenda (BJH) methods.

2.4. Assembly of supercapacitor test cells

The supercapacitor test cell was fabricated using symmetric two-electrode configuration. The working electrode was prepared by mixing the active carbon material with polyvinylidene fluoride (PVDF) binder in a 10:1 weight ratio, without incorporating any external conductive additives. The mixture was homogenized until a uniform consistency was achieved and then coated onto a circular stainless steel current collector with a diameter of 9 mm. The mass loading of the carbon material was standardized at 9 mg. The assembled system was designed to operate without the need for a separate counter electrode, enabling direct evaluation of the material performance.

2.5. Electrochemical performance test

The electrochemical performance of the supercapacitor, using oxygen-functionalized carbon nanofiber as the active material, was evaluated in a 1 M H_2SO_4 electrolyte. The analysis included cyclic voltammetry (CV, instrument: CV UR-Rad-Er 2810) and galvanostatic charge-discharge (GCD, instrument: CD UR-Rad-Er 2018) methods, as established in previous studies. A two-electrode symmetric configuration, free of external conductive additives, was used to characterize the materials performance and demonstrate potential application. CV tests were conducted at scan rates ranging from 1 to 10 mV/s, while GCD tests were performed at current densities between 1 and 10 A/g over a potential window of 0 to 1 V. The electrochemical behavior was quantitatively assessed in terms of specific capacitance, energy density, and power density. Standardized equations for symmetrical supercapacitor systems were applied to calculate these parameters, consistent with the analysis of porous carbon-based electrode materials [26,27]

3. Results and Discussion

To evaluate the phase structure and crystallinity of the hierarchical carbon nanofiber synthesized from kulim wood through impregnation and high-temperature pyrolysis, X-ray diffraction in powder analysis was conducted, as shown in Fig. 1(a). XRD pattern of the carbon material showed two broad diffraction peaks at 24° and 43°, corresponding to the (0 0 2) and (1 0 1) planes of graphite, respectively. The broad and low-intensity nature of the (0 0 2) reflection indicates a lack of long-range graphitic order, reflecting the intrinsically amorphous character of biomass-derived carbon pyrolyzed at high temperature. This peak broadening is associated with highly disordered carbon layers, interlayer spacing variation, and structural defects introduced during thermal treatment and chemical activation. Importantly, this disordered carbon structure is not detrimental but rather beneficial for electrochemical energy storage, as it introduces abundant defect sites, edge planes, and expanded interlayer spacing that facilitate electrolyte ion access and charge accommodation [28]. This indicates is commonly observed in carbon materials derived from biomass solid waste [29]. The (1 0 1) reflection plane, on the other hand, is attributed to the hexagonal carbon structure present in the precursor material [30]. The presence of these two planes suggests a highly disordered carbon framework in the synthesized material, due to the chemical reaction between KOH and the precursor at high temperatures [31]. Furthermore, the interlayer spacing of the (0 0 2) plane was measured at 0.401 nm, approximately 14% higher than conventional graphite [32]. This increase reflects the predominantly amorphous nature of the material. The interlayer spacing of the (1 0 1) plane, recorded at 0.202 nm, is in line with values reported in previous studies. The $L_c/_a$ dimension was determined to be 0.81, indicating the potential for abundant layer formation in the synthesized material. Such enlarged interlayer distances reduce steric hindrance during ion insertion and extraction, enabling faster ion transport kinetics, particularly under high current densities [29].

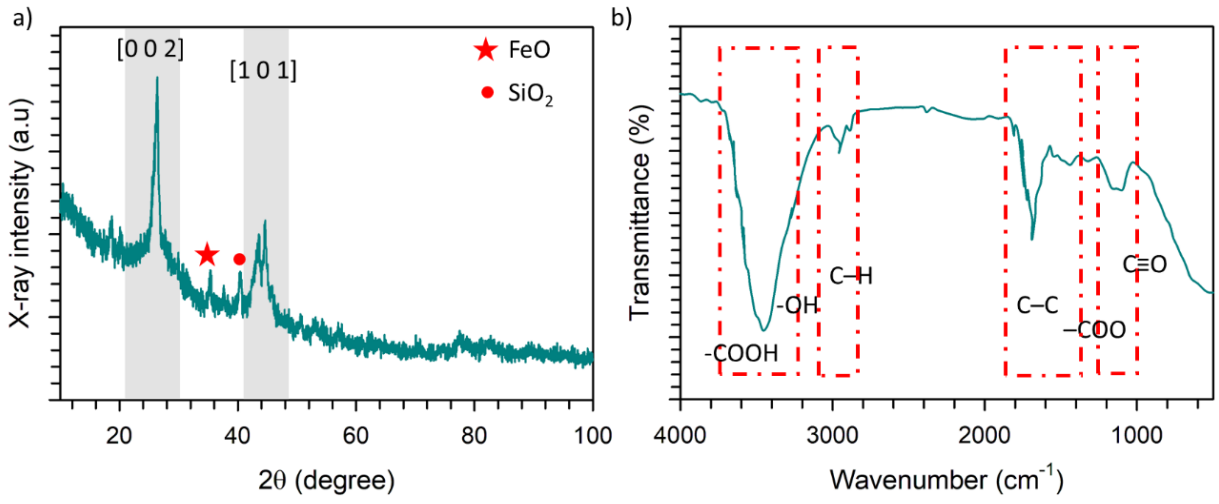

Fig. 1. (a) XRD pattern, and (b) IR spectra of porous carbon from kulim wood

Aside from the primary diffraction peaks, sharp weak peaks were observed at 34° and 37°, likely associated with the presence of inorganic compounds such as FeO and SiO_2. The presence of zinc oxide was attributed to zinc-containing impurities in the raw materials oxidized during pyrolysis, while silicon oxide originated from residues of high-temperature combustion. Although present in negligible amounts, these oxygen-containing inorganic species may contribute indirectly to the formation of surface oxygen functionalities during activation and pyrolysis, which have been reported to enhance electrode–electrolyte interaction and pseudocapacitive behavior. Recent literature consistently highlights that oxygen-rich defect sites generated through such activation pathways play a crucial role in improving charge storage efficiency and power performance in carbon-based supercapacitors [33].

To confirm the presence of oxygen functional groups in the as-prepared carbon materials, FT-IR spectroscopy was conducted, as shown in Fig. 1b. FTIR spectra showed that the synthesized materials had well-defined oxygen functionalities in the wavenumber range of 4500–500 cm^{-1}. Specifically, the stretching vibrations of oxygen-containing groups such as -COOH and -OH were observed in the range of 3600–3200 cm^{-1} [34]. A band at approximately 2921 cm^{-1} was attributed to the C–H stretching vibration. Furthermore, the vibrations of C=O, C–C, C–O, and C≡O groups were identified at bands corresponding to 1699, 1240, and 1014 cm^{-1}, respectively [35,36]. A weak stretching vibration of the C–S bond was also observed at approximately 1109 cm^{-1}. These results confirm the presence of oxygen functional groups in the synthesized carbon materials, consistent with the assumptions derived from XRD patterns discussed earlier. The presence of oxygen functional groups plays a significant role in enhancing the performance of the electrodes in energy storage systems. Oxygen functional groups contribute to improved wettability, electrical conductivity, and hydrophilicity of the working electrodes. The groups facilitate redox reactions in the charge transfer system, thereby introducing pseudocapacitive behavior in supercapacitor. This underscores the potential of the as-prepared carbon materials for advanced energy storage applications. It should be noted that FTIR analysis in this study is employed for qualitative identification of surface functional groups rather than definitive or quantitative confirmation. Although the broad and overlapping bands commonly observed in amorphous carbons limit precise functional group assignment, the presence of characteristic absorption features provides indicative evidence of oxygen-containing functionalities introduced during KOH-assisted activation. These FTIR features are consistent with well-established reports on biomass-derived activated carbons and align with the expected surface chemistry resulting from high-temperature chemical activation.

The surface morphology of the synthesized porous carbon material, derived from kulim wood waste, was inspected using SEM at appropriate magnifications. Fig. 2(a–d) show the formation of abundant carbon nanoscales through the use of an integrated chemical catalyst along with pyrolysis of kulim wood. This process led to a network of interconnected nanofibers that created rich pores in the carbon framework.

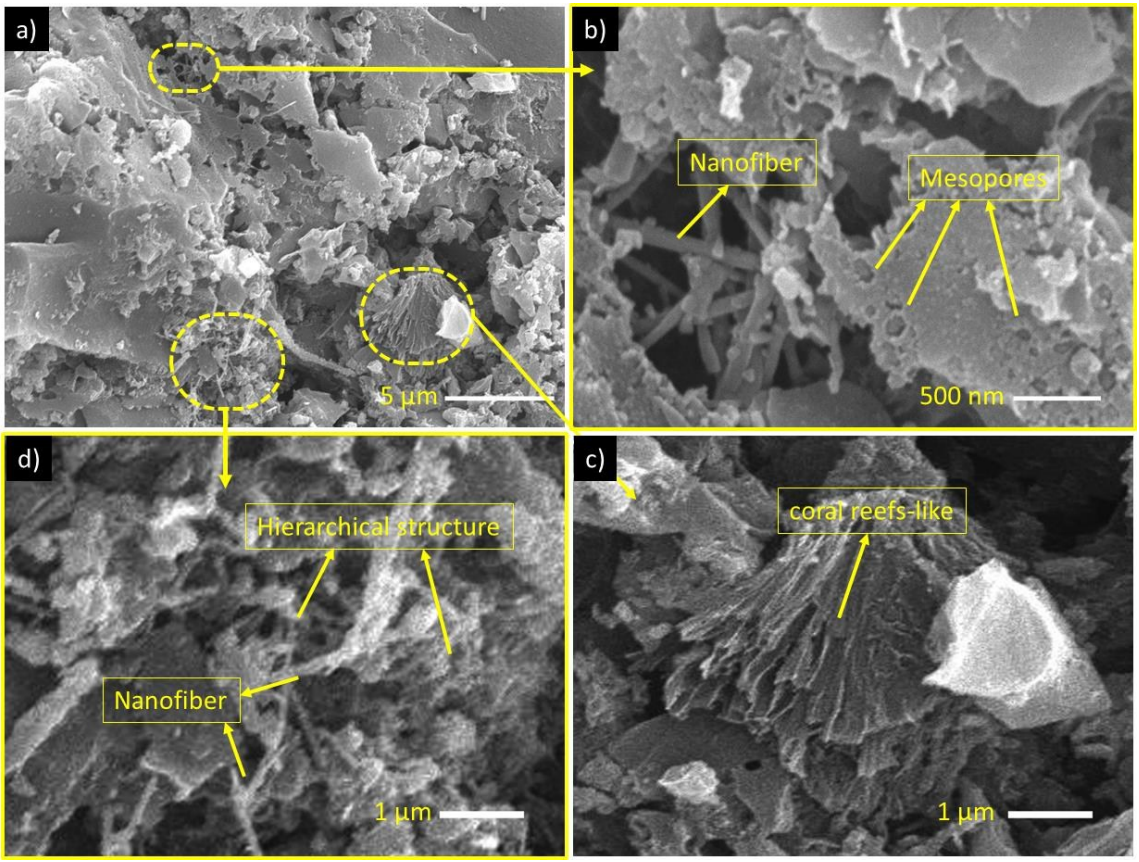

Fig. 2. Image SEM in (a) 5µm, (b) 500 nm, (c)-(d) 1 µm of porous carbon from kulim wood

By using an integrated chemical catalyst and pyrolysis, the surface structure of the synthesized carbon nanoflakes was thoroughly characterized. The integrated pyrolysis, conducted in N_2 and CO_2 environments, enabled optimal decomposition of the complex compounds present in the raw material, facilitating the development of a strong carbon framework. Kulim wood, which has a high lignocellulose content, was decomposed under a flow of N_2 gas in the furnace tube. Hemicellulose was fully decomposed, leaving behind thinly eroded cellulose, which contributed to the formation of nanofibers in the material [37,38]. The degraded lignin content in N_2 and CO_2 conditions allowed for the establishment of a solid carbon framework. The chemical catalyst, potassium KOH, starts to react at temperatures of 600°C and above, promoting extensive etching of the carbon chains in the precursor material [39]. This reaction leads to the formation of a carbon structure characterized by abundant pores and a three-dimensional hierarchical connectivity [40], as depicted by SEM image in Fig. 2(a). The precursor structure features a smooth surface punctuated by clearly visible holes, indicating the development of micro and mesoscale pores. At the 1-micron scale (Fig. 2(b)), it becomes apparent that carbon chunks are interconnected by nanofibers, with these chunks covered in pores ranging from 45 to 347 nanometers. At the same scale, a pore structure resembling coral reefs, with overlapping internal reticulation, was also observed (Fig. 2(c)). This unique morphology can improve the specific surface area, thereby enhancing electrochemical performance. In the 500-nanometer scale (Fig. 2(d)), the prepared carbon materials showcase well-defined nanofiber structures whose tops are filled with narrow pores. This observation confirms that the materials possess a three-dimensional hierarchical structure rich in pore-containing nanofibers. The distinctive structure provides a high surface area, numerous active sites, fast accessibility, and high conductivity for the working electrode.

The porosity characteristics, including pore distribution, surface area, and pore size ratio of carbon materials derived from kulim wood catalyzed by KOH during integrated pyrolysis, were investigated using N_2 sorption isotherm analysis. The isotherm curve presented in Fig. 3(a) shows a type IV adsorption profile, characterized by a typical H4 hysteresis loop, indicating the coexistence of microporosity and mesoporosity in the structure of the synthesized carbon material [41]. At lower relative pressures, the sharp initial increase in the isotherm profile reflects the abundant presence of narrow micropores [42]. Based on the t-plot analysis, the micropore surface area was calculated to be 754.174 m^2/g. The contribution of micropores is crucial in providing active sites for charge storage, enabling high charge retention and resulting in superior energy density [43]. In contrast, the H4 hysteresis loop signifies multilayer adsorption in larger, stable pores, confirming the presence of well-defined mesoporosity [44]. This observation is in line with the assumptions derived from SEM analysis discussed earlier. Using BJH method, the mesopore surface area was determined to be 316.718 m^2/g. The detailed pore size distribution, as illustrated in Fig. 3(b), shows mesopores ranging from 3.1 nm to 27 nm. Mesopores are particularly significant for electrode substrates due to the contribution to rapid ion accessibility, unimpeded charge insertion/extraction, and stable charge transport under high current densities [45].

Furthermore, BET analysis showed that the specific surface area of the as-prepared carbon material reached 1070.89 m^2/g, indicating the potential for high energy storage capacity in energy storage devices. The dual porosity system, with a micropore-to-mesopore ratio of approximately 4:1, demonstrates a synergistic effect that enhances the overall energy storage performance of the supercapacitor [46]. The high porosity of the synthesized carbon material can be attributed to the catalytic effect of KOH during the integrated pyrolysis process. KOH catalyst facilitates the creation of micropores by releasing K ions, leaving behind micro-sized voids [47]. Simultaneously, the pyrolysis process in the presence of CO_2 etches the carbon matrix, expanding narrow pore gaps into larger, well-defined mesopores. The combination of micropores and mesopores in the carbon material offers significant advantages for supercapacitor electrodes by improving the material capacity to store electrical energy while maintaining high power density [48]. This dual-scale porosity ensures optimal charge storage and transport, making the material highly suitable for advanced energy storage applications.

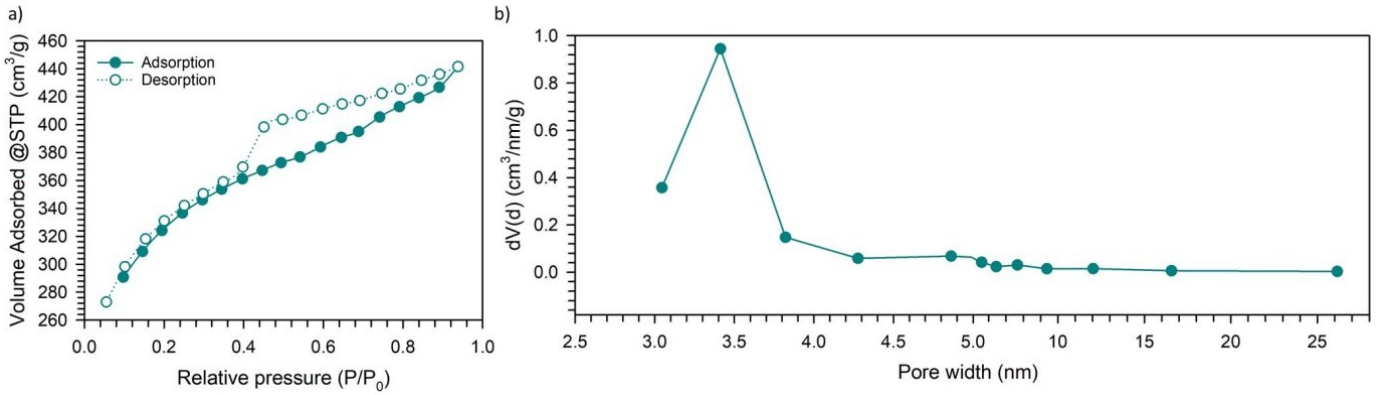

Fig. 3. (a) N_2 gas sorption isotherm, and (b) pore size distribution of porous carbon from kulim wood

The prepared carbon material exhibits high purity, characterized by a detailed ratio of oxygen functionality, with a minimal content of inorganic elements. To confirm this, an in-depth analysis of the EDS spectra is needed, as illustrated

in Fig. 4. The spectra indicate that the synthesized material contains 86.22% carbon, demonstrating the effectiveness of the method used on the precursor in producing high-purity carbon materials. Additionally, the oxygen content was recorded at 9.34%, which positively influences the electro-adsorption and desorption processes during supercapacitor operation. The oxygen atoms can interact with the active surface of the carbon material through hydrogen bonds or Van der Waals forces, facilitating a reversible effect in the charge and discharge processes of the supercapacitor. Iron (Fe) was present at 2.35%, likely derived from the biomass of kulim wood. Previous studies have shown that the presence of iron can serve as a dopant, contributing to a pseudocapacitance effect in the material. Other inorganic elements were detected in low quantities, such as aluminum (Al) at 1.06% and silicon (Si) at 1.04%. This result supports the presence of SiO_2, as previously discussed in XRD analysis. Although trace amounts of other inorganic substances are present in the prepared materials, no significant adverse effect was observed on the performance of the carbon electrode, as demonstrated in the subsequent electrochemical results.

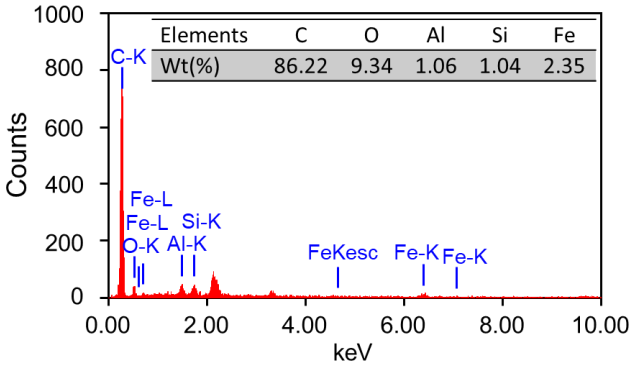

Fig. 4. EDS spectra of porous carbon from kulim wood

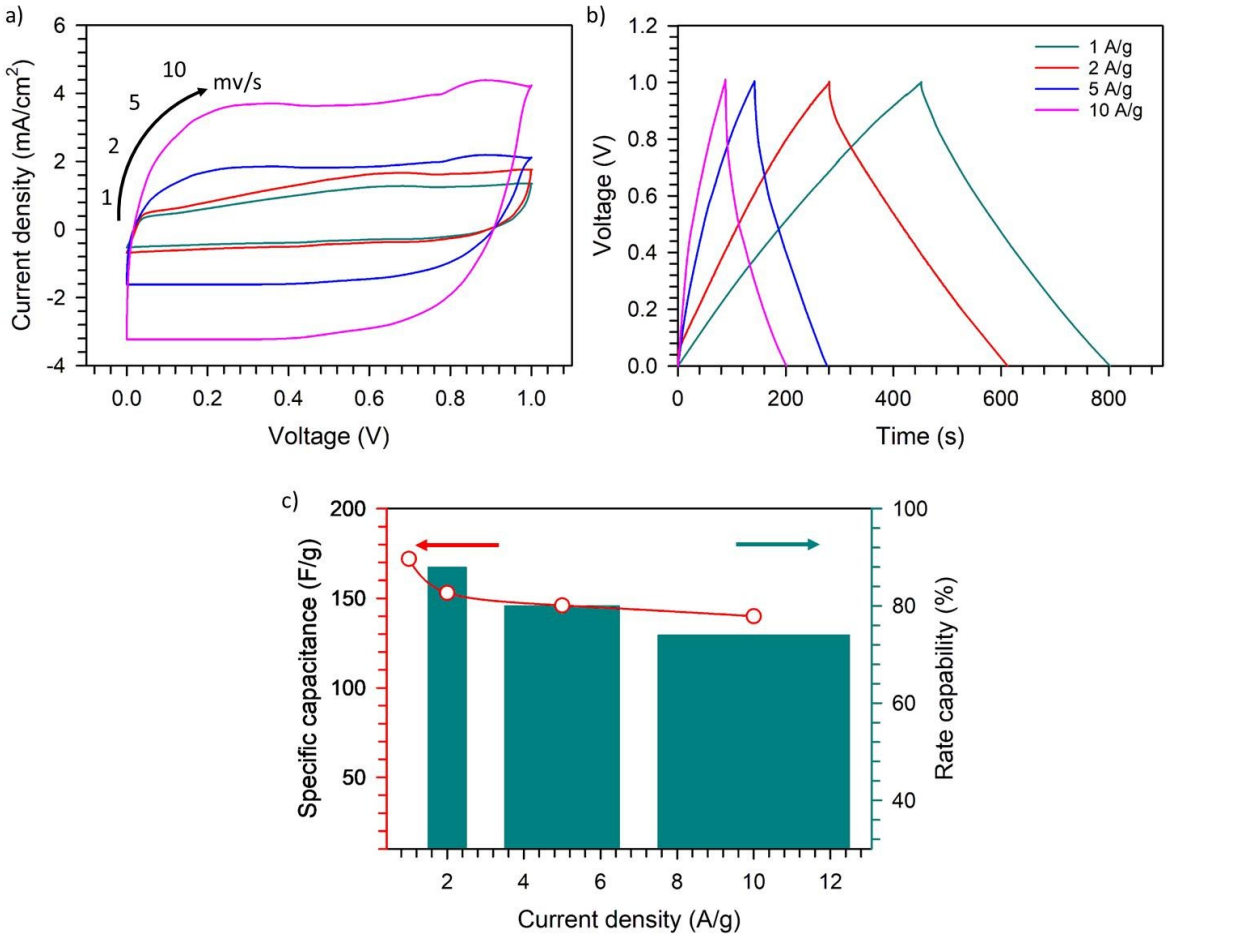

Fig. 5. (a) CV profile, (b) GCD profile, and (c) Rate capability for porous carbon from kulim wood

The electrochemical assets of symmetric supercapacitor were further analyzed through GCD measurements over a specific time scale, as shown in Fig. 5(b). GCD profiles were recorded at various current densities ranging from 1 to 10 A/g. All profiles showed nearly symmetrical isosceles triangular shapes with slight distortions, representing the domination of electric double-layer (EDL) capacitive followed by charge degradation effects, which contribute to the observed capacitance behaviour [52]. This observation is consistent with the results from CV analysis. The oxygen functionalities in the synthesized kulim wood-derived carbon materials played a substantial role in enhancing redox reactions, hydrophilicity, and wettability in the working electrodes. Therefore, the capacitive reached 172 F/g at 1 A/g, with an impressively low internal resistance (IR drop) of 0.04 Ω. This performance surpasses previous studies on commercial carbon sources combined with melamine-formaldehyde resin, which achieved a specific capacitance of only 145 F/g [1]. The

exceptional capacitive behavior can be attributed to the significant material properties of kulim wood-derived carbon. These properties include a high surface area dominated by abundant microporosity (approximately ¾ of the total S_{BET}), a hierarchical nanofiber pore structure, and the redox activity of oxygen functionalities. The abundant micropores provide extensive charge storage space, facilitating the formation of more electric double layers [53]. Meanwhile, the hierarchical nanofiber structure enhances accessibility and charge transport, enabling efficient charge diffusion [54]. The oxygen functionalities also improve hydrophilicity and wettability, further enhancing the current response of the working electrode [18]. The synergistic effects of these material properties result in outstanding capacitive performance for kulim wood-based carbon electrodes. This performance is further validated by GCD responses at higher current densities, as shown in Fig. 5(c). Although the specific capacitance decreased with increasing current density, a common behavior for solid bio-organic-based carbon materials, the electrode maintained a high-rate capability. At 10 A/g, the specific capacitance remained at 140 F/g, corresponding to an 81% retention of the initial capacitance at 1 A/g. Although micropores contribute approximately 70% of the total surface area, the carbon material maintains an excellent rate capability, retaining about 81% of its capacitance at 10 A g^{-1}. This behavior arises from the synergistic effect of a hierarchical pore architecture and surface chemistry. The interconnected mesopores function as ion-buffering reservoirs and rapid transport pathways, enabling efficient electrolyte access to microporous regions and minimizing ion diffusion resistance under high current operation. Furthermore, the dominant micropores fall within an ion-accessible size range, allowing partial desolvation and rapid formation of the electric double layer. The presence of oxygen functional groups further enhances surface wettability and reduces interfacial resistance, collectively facilitating fast charge–discharge kinetics. Consistent with these structural features, the charge-storage mechanism is dominated by surface-controlled electric double-layer capacitance, which inherently supports high-rate performance. Additionally, the high conductivity of the material from nanofiber structure, supports efficient charge transport. These factors collectively ensure excellent electrochemical performance and rate capability, making kulim wood-derived carbon a capable applicant for high-performance supercapacitor.

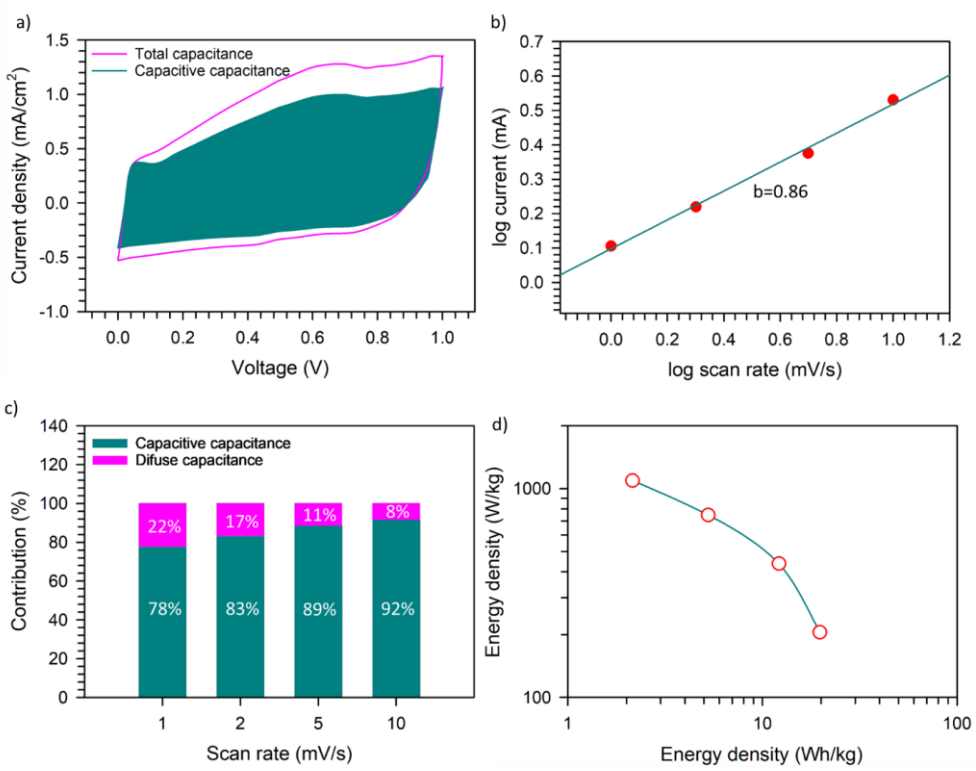

Fig. 6. (a) surface control in capacitive behavior at 1mV/s, (b) Logarithmic plot of peak current vs sweep rates, (c) capacitance contribution, and (d) Ragone plot of porous carbon from kulim wood

A comprehensive analysis of oxygen functionality effect on the electrochemical kinetics of the working electrode was conducted using the Dunn method [55], focusing on the oxidation reaction peaks observed in the voltammetry diagrams. Using the equations associated with this method, the prepared material demonstrated a combined pseudocapacitive behavior governed by both surface-controlled and diffusion-controlled mechanisms. The outcomes presented that the total capacitive conduct of the material was predominantly surface-controlled, as shown in Fig. 6(a). At a sweep rate of 1 mV/s, the capacitive-contribution was recorded at 78%, while the diffusion-controlled contribution accounted for 22%. This result confirms that oxygen functionalities significantly influence the material capacitive behavior, leading to a mixed charge storage mechanism. It is important to note that the contribution of oxygen functionalities to pseudocapacitance is governed not only by the total oxygen content, but also by the

type, distribution, and electrochemical accessibility of the functional groups. In this work, although the oxygen content (9.34 at%) is lower than that reported in some oxygen-rich carbons, the hierarchical micro–mesoporous structure ensures efficient exposure of redox-active oxygen sites to electrolyte ions, resulting in a measurable diffusion-controlled pseudocapacitive contribution (~22%). The analysis was further corroborated by the slope characteristics of the log(i) vs. log(v) plot, where the constant b-value was determined to be 0.86 (Fig. 6(b)). This b-value indicates a diverse influence to the capacitive properties (surface-controlled and diffusion-controlled behaviors). Using the Dunn method [56], the capacitive contributions were studied at varying sweep rates, as presented in Fig. 6(c). The results showed an increase in surface-controlled capacitance, rising from 78% at lower to 92% at higher sweep rates. This trend suggests that the high adsorption process at the electrode surface facilitates the creation of a rich electrical bi-layer capacitance, enhancing the electrode performance in high-current applications. Conversely, the diffusion-controlled capacitance diminished at higher sweep rates, particularly at 10 mV/s, indicating the delayed diffusion contributions of oxygen functionalities. This behavior is indicative of the transition in charge storage mechanisms, where surface-controlled processes dominate at higher sweep rates due to the speedy in/de-sertion dynamics, while diffusion processes become less significant. The synergy between surface-controlled and diffusion-controlled mechanisms, influenced by oxygen functionalities, accentuates the possible of kulim wood-derived carbon sources for application in high-performance supercapacitor, particularly under varying current conditions.

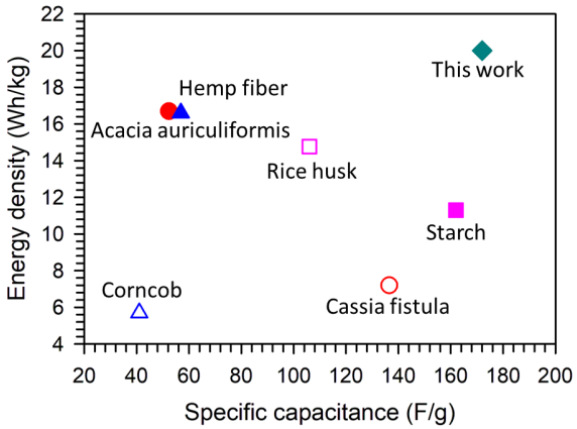

Fig. 7. Comparison of specific capacitance and energy density with other carbon biomass based

The final electrochemical concert of the fabricated symmetrical supercapacitor was evaluated through the energy and power outputs, as represented by the Ragone plot revealed in Fig. 6(d). The oxygen-functionalized carbon-based electrode had an energy output of 19.91 Wh/kg at a power output of 203 W/kg when tested at 1 A/g. At 10 A/g, the device demonstrated a maximum power output of 1.02 kW/kg, accompanied by an energy density of 2.1 Wh/kg. These feature characteristics are significantly superior to those conveyed in previous studies, particularly for symmetric electrode systems. As shown in Fig. 7, the capacitive performance and energy output values achieved in this work have been compared with added biomass-derived carbons, including starch [40], *Acacia auriculiformis* [57], *Cassia fistula* [58], hemp fiber [59], corncob [60], and rice husk [61]. It should be noted that performance superiority is not solely determined by specific capacitance. Although some reported materials exhibit higher capacitance values (>260 F g^{-1}), such values do not necessarily translate into higher energy density due to limitations in operating voltage and charge–discharge kinetics. In contrast, despite delivering a moderate capacitance of 172 F g^{-1}, the present electrode achieves a substantially higher energy output, as clearly illustrated in the Fig. 7, indicating a more balanced energy–capacitance performance. The comparison underscores the exceptional properties of the hierarchical oxygen-functionalized carbon nanofibers synthesized from kulim wood waste. These outcomes underscore the probable of the quantifiable as a sustainable and high-concert electrode for advanced supercapacitor applications.

4. Conclusion

In conclusion, this study emphasized the potential of porous carbon derived from kulim wood left-over as an cathode/anode substantial for symmetric supercapacitor. This is achieved through the combination of a hierarchical nanofiber structure and oxygen functionality. Using a one-step integrated chemical-physical synthesis method comprising KOH and CO_2, the material obtained contains well-defined oxygen functionalities, such as C–O and –COO, with an oxygen ratio of 9.34%. The hierarchical porosity structure, which included micro and mesoporosity in a ratio of 4:1, had a porosity of 1070 m^2/g. This structure facilitates a uniform distribution of the dense nanofibers, significantly enhancing the material capacitive properties. The material demonstrated a capacitive behaviour of 172 F/g at an acid electrolyte solution, along with impressive capacitance retention of 81.2% at a high current of 10 A/g. Additionally, it had a low internal resistance of 0.04 Ω, indicating excellent electrical conductivity. Analysis of the storage mechanism showed a combination of surface (83%) and diffusion control (22%), both of which contribute to energy storage efficiency. This material achieved an energy output of 19.91 Wh/kg, with a maximum power output of 1.02 kW/kg. The integration of oxygen functionality and a hierarchical nanofiber structure in activated carbon from kulim wood waste significantly enhanced the electrochemical performance of symmetric supercapacitor. Therefore, this study arranges a solid substance for the expansion of sustainable supercapacitor and contributes to biomass-based clean energy resolutions.

Acknowledgements

The research was funded by the Kementerian Pendidikan Tinggi, Sains dan Teknologi, Republic of Indonesia, under the Fundamental Research Scheme 2025, Contract No. 19521/UN19.5.1.3/AL.04/2025.

References

1. I.E. Agency, World Energy Outlook 2024, 2024.

2. A. Shuja, H.R. Khan, I. Murtaza, S. Ashraf, Y. Abid, F. Farid, F. Sajid, Supercapacitors for energy storage applications: Materials, devices and future directions: A comprehensive review, J. Alloys Compd. 1009 (2024) 176924.
3. J. Zhang, M. Gu, X. Chen, Supercapacitors for renewable energy applications: A review, Micro Nano Eng. 21 (2023) 100229.
4. H. Hu, M. Yan, J. Jiang, A. Huang, S. Cai, L. Lan, K. Ye, D. Chen, K. Tang, Q. Zuo, Y. Zeng, W. Tang, J. Fu, C. Jiang, Y. Wang, Z. Yan, X. He, L. Qiao, Y. Zhao, A state-of-the-art review on biomass-derived carbon materials for supercapacitor applications: From precursor selection to design optimization, Sci. Total Environ. 912 (2024) 169141.
5. Q.Z. Zhang, D. Zhang, Z.C. Miao, X.L. Zhang, S.L. Chou, Research Progress in MnO2–Carbon Based Supercapacitor Electrode Materials, Small 14 (2018) 1–15.
6. M.G. Tadesse, A.S. Ahmmed, J.F. Lübben, Review on Conductive Polymer Composites for Supercapacitor Applications, J. Compos. Sci. 8 (2024) 53.
7. V. Kavan Kumar, N.L. Panwar, A review on porous carbon synthesis processes and its application as energy storage supercapacitor, J. Indian Chem. Soc. 101 (2024) 101231.
8. L. Liu, W. Zhang, B. Lu, Z. Cheng, H. Cao, J. Li, Z. Fan, X. An, Controllable heteroatoms doped electrodes engineered by biomass based carbon for advanced supercapacitors: A review, Biomass and Bioenergy 186 (2024) 107265.
9. N. Sangtong, T. Chaisuwan, S. Wongkasemjit, H. Ishida, W. Redpradit, K. Seneesrisakul, U. Thubsuang, Ultrahigh-surface-area activated biocarbon based on biomass residue as a supercapacitor electrode material: Tuning pore structure using alkalis with different atom sizes, Microporous Mesoporous Mater. 326 (2021) 111383.
10. Z. Kang, D. Xu, L. Zhao, D. Liu, Boosting supercapacitor performance with high-specific surface area porous carbon derived from sugarcane bagasse, J. Energy Storage 104 (2024) 114718.
11. D. Liu, T. Guo, D. Xu, G. Xu, Z. Wang, B. Fan, Y. Ding, Rational construction of hierarchical porous carbon with ultrahigh specific surface area and rich heteroatoms toward high-performance supercapacitors, Vacuum 215 (2023) 112374.
12. X. Ni, Y. Zhao, P. Cai, Q. Xu, D. Li, Biomass-tar-derived oxygen-enriched porous carbon as a high-performance carbon electrode material for double electric layer and zinc-ion hybrid supercapacitor, Diam. Relat. Mater. 148 (2024) 1–10.
13. Q. Wang, H. Zheng, Y. Zhang, Y. Huang, W. Li, W. Huang, J. Xiang, P. Yuan, H. Xue, S. Wang, Y. Zhou, W. Lu, Biomass-based porous carbon from trachycarpus fortunei silk with the hierarchical oxygen-enriched structure for high performance flexible all-solid-state supercapacitor, J. Phys. Chem. Solids 185 (2024) 111785.
14. Atika, R.K. Dutta, Oxygen-rich porous activated carbon from eucalyptus wood as an efficient supercapacitor electrode, Energy Technol. 9 (2021) 1–12.
15. K. Al, S. Başakçılardan Kabakcı, Oxygen-rich precursors via glycerol organosolv treatment: Preparation of activated carbon from hazelnut shell and its structural components for possible use in electrodes for supercapacitors, Int. J. Thermofluids 21 (2024) 100588.
16. S. Zhong, L. Dai, H. Xu, C. Yuan, S. Wang, Biomorphic porous carbon derived from reed with enriched oxygen-functional groups for high-performance supercapacitors, Diam. Relat. Mater. 141 (2024).
17. X. Geng, G. Singh, C.I. Sathish, Z. Li, R. Bahadur, Y. Liu, S. Li, X. Yu, M. Breese, J. Yi, A. Vinu, Biomass derived nanoarchitectonics of porous carbon with tunable oxygen functionalities and hierarchical structures and their superior performance in CO2 adsorption and energy storage, Carbon N. Y. 214 (2023).
18. Z. Chen, Y. Chen, Q. Wang, T. Yang, Q. Luo, K. Gu, W. Yang, Molecularly-regulating oxygen-containing functional groups of ramie activated carbon for high-performance supercapacitors, J. Colloid Interface Sci. 665 (2024) 772–779.
19. X. Wang, B. Liu, S. Wang, H. Xie, Y. Zha, X. Huang, D.M.F. Santos, Y. Li, Oxygen self-doped hierarchical porous carbons derived from coal liquefaction residue for high-performance supercapacitors in organic and ionic liquid-based electrolytes, Colloids Surfaces A Physicochem. Eng. Asp. 669 (2023) 131552.
20. E. Taer, N. Nursyafni, A. Apriwandi, A. Fudholi, N. Chitraningrum, M. Deraman, R. Taslim, Oxygen-functionalization of unique hierarchical carbon nanosheet fishtail-like for synergistically enhanced capacitive performance supercapacitor, Adv. Nat. Sci. Nanosci. Nanotechnol. 15 (2024) 045011.
21. E. Taer, L. Pratiwi, Apriwandi, W.S. Mustika, R. Taslim, Agustino, Three-dimensional pore structure of activated carbon monolithic derived from hierarchically bamboo stem for supercapacitor application, Commun. Sci. Technol. 5 (2020) 22–30.
22. E. Taer, F. Hasanah, R. Taslim, Nanofiber-enrich activated carbon coin derived from tofu dregs as electrode materials for supercapacitor, Commun. Sci. Technol. 6 (2021) 41–48.
23. W.M. Nursyaputri, Z.K. Fairuzy, Z. Khumairah, N. Yanti, N. Nursyafni, A. Apriwandi, R. Taslim, E. Taer, Novel colored biomass-waste from food industry sector derived hierarchical porous carbon nanofiber for robust symmetric supercapacitor, Commun. Sci. Technol. 9 (2024) 411–420.
24. I. Ali, M. Asim, T.A. Khan, Low cost adsorbents for the removal of organic pollutants from wastewater, J. Environ. Manage. 113 (2012) 170–183.
25. J. Khajonrit, T. Sichumsaeng, O. Kalawa, S. Chaisit, A. Chinnakorn, N. Chanlek, S. Maensiri, Mangosteen peel-derived activated carbon for supercapacitors, Prog. Nat. Sci. Mater. Int. 32 (2022) 570–578.
26. S. Huang, D.D. Ma, X. Wang, Y. Shi, R. Xun, H. Chen, H. Guan, Y. Tong, A space-sacrificed pyrolysis strategy for boron-doped carbon spheres with high supercapacitor performance, J. Colloid Interface Sci. 608 (2022) 334–343.
27. D. Zhang, W. Ma, K. Li, Manipulating internal morphology and mesoporous in monodisperse carbon nanospheres for supercapacitor with organic electrolyte, J. Energy Storage 91 (2024) 112114.
28. B. Gorji, A. Khosrozadeh, S. Doja, L. Tao, M.B. Miller, L. Bichler, M. Arjmand, J. Liu, Critical evaluation of hybrid and organic electrolytes for supercapacitors with optimized porous carbon, Electrochim. Acta 441 (2023) 141778.
29 R. Sun, Y. Chen, X. Gao, G. Xie, R. Yang, C. Yang, Y. Shi, Y. Yi, Sodium lignosulfonate-derived hierarchical porous carbon electrode materials for supercapacitor applications, J. Energy Storage 91 (2024) 112025.
30. L. Wang, W. Li, P. Li, L. Zhang, L. Li, KHCO3 chemical-activated hydrothermal porous carbon derived from jackfruit inner skin for supercapacitor applications, J. Mol. Struct. 1318 (2024) 139380.
31. B. Tekin, Y. Topcu, Novel hemp biomass-derived activated carbon as cathode material for aqueous zinc-ion hybrid supercapacitors: Synthesis, characterization, and electrochemical performance, J. Energy Storage 77 (2024) 109879.
32. J. Serafin, M. Baca, M. Biegun, E. Mijowska, R.J. Kaleńczuk, J. Sreńscek-Nazzal, B. Michalkiewicz, Direct conversion of biomass to nanoporous activated biocarbons for high CO2 adsorption and supercapacitor applications, Appl. Surf. Sci. 497 (2019) 143722.
33. K. Chen, S. Weng, J. Lu, J. Gu, G. Chen, O. Hu, X. Jiang, L. Hou, Facile synthesis of chitosan derived heteroatoms-doped hierarchical porous

carbon for supercapacitors, Microporous Mesoporous Mater. 320 (2021) 111106.
34. C.F. Xue, Y. Lin, W. Zhao, T. Wu, Y.Y. Wei, X.H. Li, W.J. Yan, X.G. Hao, Green preparation of high active biochar with tetra-heteroatom self-doped surface for aqueous electrochemical supercapacitor with boosted energy density, J. Energy Storage 90 (2024) 111872.
35. T. Wang, F. Yin, Y. Fang, C. Sun, Waste Cigarette Butts-Derived Nitrogen-Doped Carbon Fibers Loaded with Ru Nanoparticles as an Efficient Cathode Catalyst for Lithium-Oxygen Batteries, ACS Sustain. Chem. Eng. 11 (2023) 9163–9171.
36. M. Jayachandran, A. Rose, T. Maiyalagan, N. Poongodi, T. Vijayakumar, Effect of various aqueous electrolytes on the electrochemical performance of α-MnO2 nanorods as electrode materials for supercapacitor application, Electrochim. Acta 366 (2021) 137412.
37. R. Farma, I. Apriyani, A. Awitdrus, E. Taer, A. Apriwandi, Hemicellulosa-derived Arenga pinnata bunches as free-standing carbon nanofiber membranes for electrode material supercapacitors, Sci. Rep. 12 (2022) 2572.
38. S.R.A. Sasono, M.F. Rois, W. Widiyastuti, T. Nurtono, H. Setyawan, Nanofiber-enrich dispersed activated carbon derived from coconut shell for supercapacitor material, Results Eng. 18 (2023) 101070.
39. Y. Zhao, J. Mu, Y. Wang, Y. Liu, H. Wang, H. Song, Preparation of hierarchical porous carbon through one-step KOH activation of coconut shell biomass for high-performance supercapacitor, J. Mater. Sci. Mater. Electron. 34 (2023) 1–22.
40. Z. Zhai, S. Wang, Y. Xu, L. Zhang, X. Wang, H. Yu, B. Ren, Starch-based carbon aerogels prepared by an innovative KOH activation method for supercapacitors, Int. J. Biol. Macromol. 257 (2024) 128587.
41. Y. Yao, D. Ge, Y. Yu, Y. Zhang, C. Du, H. Ye, L. Wan, J. Chen, M. Xie, Filling macro/mesoporosity of commercial activated carbon enables superior volumetric supercapacitor performances, Microporous Mesoporous Mater. 350 (2023).
42. Q. Li, Y. Jiang, Z. Jiang, J. Zhu, X. Gan, F. Qin, T. Tang, W. Luo, N. Guo, Z. Liu, L. Wang, S. Zhang, D. Jia, Z. Fan, Ultrafast pore-tailoring of dense microporous carbon for high volumetric performance supercapacitors in organic electrolyte, Carbon N. Y. 191 (2022) 19–27.
43. C. Ding, T. Liu, X. Yan, L. Huang, S. Ryu, J. Lan, Y. Yu, W.H. Zhong, X. Yang, An ultra-microporous carbon material boosting integrated capacitance for cellulose-based supercapacitors, Nano-Micro Lett. 12 (2020) 63.
44. P. Dong, K. Huo, X. Ma, X. Ma, Y. Gu, M. Lu, J. Zhang, Y. Wang, C. Zhao, Treating the wastes with wastes: Simple preparation of monolithic biomass-derived electrode for enhanced electro-Fenton treatment of pharmaceutical wastewater, Chem. Eng. J. 504 (2025) 158720.
45. Y. Yardım, İ. Genel, C. Saka, Enhanced supercapacitor performance of hierarchical mesoporous sulfur-doped carbon particles from biomass waste for energy storage, Int. J. Hydrogen Energy 99 (2025) 383–393.
46. M.K. Gabookolwe, O.R. Onisuru, S. Odisitse, R. Meijboom, C. Muiva, C.K. King'ondu, Biomass Nanoarchitectonics of abattoir waste to high coulombic efficient mesoporous carbon materials for supercapacitors, J. Energy Storage 104 (2024) 114541.
47. Y. Li, J. Mei, L. Wu, Q. Xu, Z. Li, Ultrahigh surface area hierarchical porous carbon derived from biomass via a new KOH activation strategy for high-performance supercapacitor, Int. J. Hydrogen Energy 49 (2024) 67–80.
48. A. Gopalakrishnan, S. Badhulika, Sulfonated porous carbon nanosheets derived from oak nutshell based high-performance supercapacitor for powering electronic devices, Renew. Energy 161 (2020) 173–183.
49. D. Chinnadurai, H.J. Kim, S. Karupannan, K. Prabakar, Multiscale honeycomb-structured activated carbon obtained from nitrogen-containing mandarin peel: high-performance supercapacitors with significant cycling stability, New J. Chem. 43 (2019) 3486–3492.
50. A. Gopalakrishnan, S. Badhulika, Effect of self-doped heteroatoms on the performance of biomass-derived carbon for supercapacitor applications, J. Power Sources 480 (2020) 228830.
51. C. Zhang, Q. Fan, J. Xu, M. Huang, F. Luo, D. Wang, Z. Zheng, Surface oxygen-containing functional groups: A key tradeoff in carbon-based energy storage devices, Chem. Eng. J. 505 (2025) 159162.
52. T. Li, D. Wang, B. Zhang, P. Ding, H. Li, T. Wang, Q. Pei, X. Liu, R. Guo, Tetra-heteroatom self-doped and hierarchical porous carbon toward high-performance zinc-ion hybrid supercapacitors, Chem. Eng. Sci. 298 (2024) 120352.
53. S. Liu, K. Dong, F. Guo, J. Wang, B. Tang, L. Kong, N. Zhao, Y. Hou, J. Chang, H. Li, Facile and green synthesis of biomass-derived N, O-doped hierarchical porous carbons for high-performance supercapacitor application, J. Anal. Appl. Pyrolysis 177 (2024) 106278.
54. R. Taslim, M.I. Hamdy, M. Siska, E. Taer, D.A. Yusra, M. Jelita, S. Afriani, N. Gusnita, Interconnected activated carbon nano fiber derived from mission grass for electrode materials of supercapacitor, Adv. Nat. Sci. Nanosci. Nanotechnol. 12 (2021) 35013.
55. M. Jalalah, S. Rudra, B. Aljafari, M. Irfan, S.S. Almasabi, T. Alsuwian, M.I. Khazi, A.K. Nayak, F.A. Harraz, Sustainable synthesis of heteroatom-doped porous carbon skeleton from Acacia auriculiformis bark for high-performance symmetric supercapacitor device, Electrochim. Acta 414 (2022) 140205.
56. R. Han, F. Liu, S. Geng, M. Yao, L. Luo, J. Ma, X. Wang, N,O self-doped porous carbon derived from distiller's grains for high performance supercapacitors, Ind. Crop. Prod. 214 (2024) 118550.
57. V.S. Bhat, T.J. Jayeoye, T. Rujiralai, U. Sirimahachai, K.F. Chong, G. Hegde, Acacia auriculiformis–Derived Bimodal Porous Nanocarbons via Self-Activation for High-Performance Supercapacitors, Front. Energy Res. 9 (2021) 1–15.
58. P. Rajivgandhi, A. Mariappan, M. Manivannan, R. Kumar Dharman, T. Hwan Oh, A. Sekar, Biomass waste derived from cassia fistula into value-added porous carbon electrode for aqueous symmetric supercapacitors, Inorg. Chem. Commun. 165 (2024) 1–7.
59. Y. Gao, C. Liu, Y. Jiang, Y. Zhang, Y. Wei, G. Zhao, R. Liu, Y. Liu, G. Shi, G. Wang, Hydrothermal assisting biomass into a porous active carbon for high-performance supercapacitors, Diam. Relat. Mater. 148 (2024)..
60. A. Sandeep, P. T, A. V. Ravindra, Activated carbon derived from corncob via hydrothermal carbonization as a promising electrode for supercapacitors, Mater. Res. Bull. 179 (2024) 112991.
61. N. Boonraksa, E. Swatsitang, K. Wongsaprom, Biomass nanoarchitectonics with activated rice husk char for nanoporous carbon as electrode material : Enhancing supercapacitor electrochemical performance, J. Non. Cryst. Solids 637 (2024) 123064.